Histol Histopathol (2015) 30: 601-613
DOI: 10.14670/HH-30.601

http://www.hh.um.es

Histology and Histopathology
Cellular and Molecular Biology

Assessment of murine brain tissue shrinkage caused by different histological fixatives using magnetic resonance and computed tomography imaging

Hans F. Wehrl[1], Ilja Bezrukov[1,2], Stefan Wiehr[1], Mareike Lehnhoff[1], Kerstin Fuchs[1], Julia G. Mannheim[1], Leticia Quintanilla-Martine[3], Ursula Kohlhofer[3], Manfred Kneilling[1,4], Bernd J. Pichler[1] and Alexander W. Sauter[1,5]

[1]Werner Siemens Imaging Center, Department of Preclinical Imaging and Radiopharmacy, Eberhard Karls University Tuebingen, [2]Department of Empirical Inference, Max-Planck-Institute for Intelligent Systems, [3]Department of Pathology, Eberhard Karls University Tuebingen, [4]Department of Dermatology, Eberhard Karls University Tuebingen and [5]Department of Diagnostic and Interventional Radiology, Eberhard Karls University Tuebingen, Tuebingen, Germany

Summary. Especially for neuroscience and the development of new biomarkers, a direct correlation between *in vivo* imaging and histology is essential. However, this comparison is hampered by deformation and shrinkage of tissue samples caused by fixation, dehydration and paraffin embedding.

We used magnetic resonance (MR) imaging and computed tomography (CT) imaging to analyze the degree of shrinkage on murine brains for various fixatives. After *in vivo* imaging using 7 T MRI, animals were sacrificed and the brains were dissected and immediately placed in different fixatives, respectively: zinc-based fixative, neutral buffered formalin (NBF), paraformaldehyde (PFA), Bouin-Holland fixative and paraformaldehyde-lysine-periodate (PLP). The degree of shrinkage based on mouse brain volumes, radiodensity in Hounsfield units (HU), as well as non-linear deformations were obtained.

The highest degree of shrinkage was observed for PLP (68.1%, $P<0.001$), followed by PFA (60.2%, $P<0.001$) and NBF (58.6%, $P<0.001$). The zinc-based fixative revealed a low shrinkage with only 33.5% ($P<0.001$). Compared to NBF, the zinc-based fixative shows a slightly higher degree of deformations, but is still more homogenous than PFA.

Tissue shrinkage can be monitored non-invasively with CT and MR. Zinc-based fixative causes the smallest degree of brain shrinkage and only small deformations and is therefore recommended for *in vivo ex vivo* comparison studies.

Key words: Imaging, Fixation, Paraffin, Shrinkage, Brain

Offprint requests to: Alexander Sauter, Werner Siemens Imaging Center, Department of Preclinical Imaging and Radiopharmacy, Eberhard Karls University Tuebingen, Roentgenweg 13, D-72076 Tuebingen, Germany. e-mail: alexander.sauter.imaging@gmail.com

Introduction

Molecular imaging allows for the *in vivo* elucidation and characterization of disease processes and mechanisms in humans and small animals, in many cases without or with only marginal interference with the underlying physiology. However, newly developed imaging biomarkers need a histopathological correlation for a comprehensive understanding and validation. This is particularly true for disease of the central nervous system.

It is well known that histological fixatives alter the tissue characteristics and cause shrinkage. Different fixation methods exist and are used. Each of them has

Abbreviations. 3V, 3rd ventricle; 4V, 4th ventricle; BC, bottom cerebellum; CT, computed tomography; F, lobes frontal lobes; GFA, glial fibrillary acidic protein; HU, Hounsfield units; IH, interhemispheric; L-R, cerebellum left and right cerebellum; MR, magnetic resonance; NBF, neutral buffered formalin; PFA, paraformaldehyde; PLP, paraformaldehyde-lysine-periodate; TE, echo time; TR, repetition time; T, lobes temporal lobes; UTE, Ultra Short Echo Time

different strengths and weaknesses (Howat and Wilson, 2014). The changes in tissue characteristics and shrinkage make an exact comparison between *in vivo* imaging techniques and *ex vivo* histological methods difficult. Regarding the frequently used formalin-based fixations, the changes in tissue parameters are caused by cross-linking between proteins, proteins and nucleic acids as well as formation of coordinate bonds for calcium ions (Werner et al., 2000). For alcohol- and acetone-based fixations, coagulation of tissue proteins is initiated (Werner et al., 2000). Zinc salts can react with tissue end-groups such as amino and carboxyl groups, forming reversible reaction products (Eltoum et al., 2001). Picric acid, a coagulation fixative, changes the charges on ionizable protein side chains and can break electrostatic and hydrogen bonds (Eltoum et al., 2001). Finally, shrinkage effects are aggravated by dehydration linked to graded alcohol solutions and paraffin embedding (Overgaard and Meden, 2000).

Especially for the brain, these fixation artifacts are complex and can be described with three-dimensional strain fields (Schulz et al., 2011). It is well known that accurate registration of magnetic resonance brain images and histology slides is difficult due to the highly convolved structures of the brain (Liu et al., 2010). During histological processing, even more stereological problems occur that complicate a co-registration of *in vivo* imaging and *ex vivo* histology (Dorph-Petersen et al., 2001). However, stereological methods are of great importance for quantitative information (Dorph-Petersen et al., 2001).

In the first five days of tissue fixation using formalin, an increase in weight and volume can be measured, followed by a steady decrease (Quester and Schröder, 1997). Applying a formalin fixation for up to 70 days post mortem to the human brain causes global volume shrinkage of 8.1% (Schulz et al., 2011). Taking the effects of dehydration and embedding in paraffin into account, volume shrinkages of 42% in the cerebellum and 45% in the cerebrum have been calculated (Gellért and Csernovszki, 1971; Quester and Schröder, 1997). These differences cause a non-linear shrinkage which is probably linked to different water and myelin contents between cerebellum and cerebrum (Quester and Schröder, 1997). This might exhibit an even more significant problem in diseased versus healthy brain regions.

Nowadays, formalin is classified as a carcinogen (Zanini et al., 2012) and regarded as toxic (Werner et al., 2000). It is associated with nasopharyngeal carcinoma and leukemia (Zanini et al., 2012). Zinc-based fixatives are more and more used as non-toxic alternatives. These agents provide superior morphology (Zanini et al., 2012) and similar DNA, RNA and protein preservations compared to formalin (Tbakhi et al., 1999; Wester et al., 2003).

The type and length of fixation causes different characteristics of brain tissue shrinkage. While the degree of shrinkage is well known for formalin, the other fixatives have not been fully characterized (Quester and Schröder, 1997). The assessment of the shrinkage degree is crucial for the correlation between *in vivo* imaging and histology. Less shrinkage and consecutively lower volume reduction can be better compensated with rigid and non-rigid co-registration algorithms. Although there is some literature regarding the effect of fixative solutions on tissue properties (Shepherd et al., 2009; Schulz et al., 2011), these studies are usually performed on non-embedded tissue, which is often not suitable for dedicated histological staining methods. Therefore, we set out to compare the impact of different tissue fixation methods on murine brains using magnetic resonance (MR) and computed tomography (CT) imaging.

Materials and methods

Animals

BALB/c mice (Charles River, Germany) with an age between 8 to 12 weeks were used for the experiments. A total of 72 animals were used; the animals were also part of other study projects. The animal studies were conducted according to the German animal protection law protocols for animal use and care and were approved by the local authorizing agency (Regierungspraesidium Tuebingen).

In vivo MR imaging

MR imaging (MRI) was performed using a 7 T small animal MR scanner (ClinScan, Bruker, Germany). The mice were anesthetized using 1.5% isoflurane vaporized in 100% oxygen (flow 1.5 L/min) and placed on a warmed animal support. A four-channel mouse brain coil was applied for signal reception. A T2-weighted turbospin-echo sequence (repetition time: TR=3,000 ms, echo time: TE=205 ms, turbo factor=161 a matrix size of 160×256×120, a voxel size of 0.22×0.22×0.22 mm^3) was used.

Brain tissue fixation, dehydration and paraffin-embedding

The animals were sacrificed after MR imaging. The mouse brains were carefully dissected and immediately placed in different immersion fixatives, respectively:

-Standard zinc-based fixative: 0.5% zinc chloride (Carl Roth, Germany), 0.5% zinc acetate (Carl Roth, Germany), 0.05% calcium acetate (Carl Roth, Germany) in 0.1 M Tris–HCl pH 6.4-6.7 (Lykidis et al., 2007).

-Neutral buffered formalin (NBF): 10% neutral buffered formalin solution (SAV LP GmbH, Germany), which has a content of 4.5% formaldehyde.

-Paraformaldehyde (PFA): 4% paraformaldehyde in 0.1 M phosphate buffer pH 7.4 made from freshly depolymerized paraformaldehyde (Sigma Aldrich, Germany) (Sakanaka et al., 1987).

-Bouin-Holland fixative: stock solution: 4% (mass concentration w/v) picric acid (Applichem, Germany),

2.5% (w/v) copper acetate (Sigma Aldrich, Germany), distilled water; working solution: 100 mL of Bouin-Holland stock solution, 10 mL of 37% paraformaldehyde solution (Sigma Aldrich, Germany), 10 mL of a saturated solution of mercury chloride (Sigma Aldrich, Germany) (Benerini Gatta et al., 2012)

-Paraformaldehyde-lysine-periodate (PLP): 8% (w/v) paraformaldehyde (Sigma Aldrich, Germany), distilled water, 0.04 M lysine in twice concentrated (i.e., 0.2 M) PBS (Merck Millipore, Germany), 0.55 g/L sodium periodate (Sigma Aldrich, Germany) (Pieri et al., 2002).

The brain tissue fixation process was continued with an ascending ethanol gradient (Sigma Aldrich, Germany) and immersion in Clear-Rite 3 (Microm, Germany). All fixation processes were carried out at room temperature. No further dedicated handling of the tissues was performed (e.g. suspension of the brain, high density fixation mixtures) to minimize gravitational effects. Finally the tissues were embedded in paraffin (Carl Roth, Germany).

As a function of the fixation type and duration the following groups were defined: Zinc-based fixative for 6 h (n=3), zinc-based fixative for 24 h (n=10), zinc-based fixative for 48 h (n=10), NBF for 48 h (n=10), PFA for 48 h (n=10), Bouin-Holland fixative for 48 h (n=10) and PLP for 48 h (n=10).

Osmolarity of the fixatives as well as of NaCl and NBF that was diluted (85% aqua, 15% NBF solution) were measured using an Osmometer (Osmomat 030, Gonotec, Germany). Each measurement was repeated three times. In addition, three animals per group were used for experiments using NaCl (48 h, instead of a fixative) and diluted NBF followed by the continuation of the fixation process and paraffin embedding as described above. In addition, a direct comparison between *in vivo* measurement with MRI and *ex vivo* measurement of the extracted brains using MRI was performed in three animals. No paraffin embedding was performed for the direct *in vivo* to *ex vivo* comparison.

Ex vivo CT imaging

Due to the loss of water by the fixation process and also the paraffin embedding, which is the main constituent for the MR signal, MR imaging was not suitable *ex vivo*. Trials of *ex vivo* MR imaging resulted in low signal to noise ratio images, which did not allow reliable determination of tissue outlines. Therefore, the embedded tissues needed to be scanned with a microCT. CT scans of the embedded samples were performed using a combined high-resolution single-photon emission computed tomography scanner (Inveon SPECT/CT, Siemens Healthcare, USA) operating with an X-ray source at 80 kVp and 500 mA tube current. Exposure time was set to 1000 ms and a binning factor of 2 was used resulting in a reconstructed isotropic pixel size of 52 μm.

Volume and density changes

Mouse brains derived from *in vivo* and *ex vivo* imaging were manually segmented using the software package Amira 5.4 (VSG, USA). Outlines of the mouse brain surface for volume determination were drawn by hand, and also based on thresholds; finally the outcome of this manual segmentation process was visually checked. Brain volumes (measured in mm^3) from MR and CT images were recorded. Fig. 1A shows an example of a segmented MR scan, Fig. 1B a CT scan after PFA fixation and Fig. 1C after zinc-based fixation. The corresponding brain three-dimensional volumes rendered from the corresponding MR and CT data are represented by Fig. 1D-F. Additionally, *ex vivo* brain tissue density (radiodensity measured in Hounsfield units: HU) was analyzed for each sample. Density values (HU) give an indication for image contrast changes caused by different fixatives.

Descriptive statistics including mean and standard deviation (SD) were calculated with JMP 8.0.2 (SAS Institute Inc., USA). Corresponding *in vivo* and *ex vivo* brain volumes of each fixation group were compared with paired Student's t-tests. Shrinkage of the brain volumes was calculated using the following equation:

$$Shrinkage = \frac{in\ vivo\ volume\ -\ ex\ vivo\ volume}{in\ vivo\ volume}$$

Shrinkage values were multiplied by 100 to yield a percentage value. Differences were considered to be significant if $P<0.05$.

Evaluation of non-linear deformations due to fixation

We performed an evaluation of non-linear deformations caused by the fixatives on 3 different fixatives (48 h NBF, 48 h PFA and 48 h zinc-based fixative), each subset including 3 datasets. Two methods were used: a landmark-based distance evaluation and an evaluation of the contour deformations using non-rigid registration.

For the landmark-based evaluation, we placed 10 landmarks in corresponding locations in the MR and CT datasets. These landmarks are shown in Fig. 4A. Specifically, they are the left and right frontal lobes (F lobes), the left and right temporal lobes (T lobes), the point between the F lobes, indicating a position at the interhemisphere (IH), the 3rd ventricle (3V), the 4th ventricle (4V), the left and right cerebellum (L-R cerebellum) and the bottom cerebellum (BC). From these 10 landmarks a total of 7 distances were computed. Four distances were in frontal - caudal direction between the 3rd ventricle and the bottom cerebellum (3V-BC), between the 4th ventricle and the interhemisphere (4V-IH), between the frontal and temporal lobes on the left side (F-T lobes left) and the frontal and temporal lobes on the right side (F-T lobes right). In addition, three distances were in the left-right direction, running from

the left to the right cerebellum (L-R cerebellum), between the left and right frontal lobes (L-R frontal lobes) and between left and right temporal lobes (L-R temporal lobes). Subsequently, mean and SD for relative differences of the distances as measured in *in vivo* MR and *ex vivo* CT images were computed, and the tissue shrinkage between *in vivo* and *ex vivo* images assessed.

For the evaluation of the contour deformations, a binary mask was applied on the *in vivo* MR and *ex vivo* CT data to remove the background and non-brain tissues. Placing the points of origin at the brain centers of gravity aligned the MR and CT datasets. Subsequently, the CT images were non-rigidly co-registered to the MR data using Statistical Parametric Mapping (SPM 8, Wellcome Department of Cognitive Neurology, University College London, http://www.fil.ion.ucl.ac.uk/spm). After registration, the lengths of deformation vectors were computed for surface voxels of the co-registered CT image. Subsequently, histograms (each including 3 datasets), quantiles (25%, 50% (median) and 75%) for the deformation vector lengths were computed. We used these non-parametric characterisations (quantiles instead of mean and SD) since the distributions appeared to be non-Gaussian.

Histology

To assure a constant quality of the histological procedures random samples were cut into 3 µm sections, stained with hematoxylin and eosin (H&E) and analyzed by two experienced pathologist (L.Q-M., U.K.). Immunohistochemistry was performed on an automated immunostainer (Ventana Medical Systems, Inc., Tucson, AZ, USA) according to the company's protocols for open procedures with slight modifications. All slides were stained with the primary monoclonal mouse antibody GFAP (glial fibrillary acidic protein; clone 6F2; Dako Deutschland GmbH; Germany; dilution 1:1000). Appropriate positive and negative controls were used to confirm the adequacy of the staining.

Results

Changes of in vivo and ex vivo brain volumes as a consequence of different fixatives

Osmolarity values for the used fixatives and for NaCl are reported in Table 1, for NaCl no significant shrinkage effect was observed (P=0.072). The *in vivo* brain volumes measured by MRI of the different experimental groups of mice ranged from 428.7 mm^3 to 495.7 mm^3 (Table 1). The *ex vivo* volumes measured by CT ranged from 150.9 mm^3 for the PLP fixative (48 h) to 358.1 mm^3 for the zinc-based fixative (6 h). The comparison between the *in vivo* brain volumes measured by MR imaging and the corresponding *ex vivo* CT brain volumes revealed a significant decrease (P<0.05) as a consequence of the fixation regardless of which fixative was used. The highest degree of shrinkage was observed with PLP (68.1%, 48 h), followed by PFA (60.2%, 48 h) and NBF (58.6%, 48 h). The zinc-based fixatives revealed a fixation time-dependency with volume reductions ranging from 16.5% (6 h) to 33.5% (48 h). An example of a segmented *in vivo* MR of a mouse brain is represented in Fig. 1A. Fig. 1B shows an *ex vivo* CT of a paraffin-embedded brain after 48 h fixation with PFA. The tissue density, indicated by an increase in brightness, is much higher after fixation with 48 h zinc-based solution (Fig. 1C). Corresponding three-dimensional rendered volumes are shown in Fig. 1D-F. The lower resolution of the MR acquisition results in a more pixelated surface of the *in vivo* volume (Fig. 1D). A direct comparison between *in vivo* brain volumes (492.9±4.5 mm^3) measured with MR and *ex vivo* brain volumes measured with MR (456.8±31.8 mm^3), revealed no significant shrinkage effect (P=0.226).

Ex vivo brain tissue densities of the different fixatives

Radiodensity values (HU) increased from -143.4 for PFA (48 h) to 60.6 for zinc-based fixative (48 h) (Table

Table 1. *In vivo* and *ex vivo* brain tissue volumes of the different fixative groups.

	Osmolarity (mOsmol/kg)		*in vivo* volumes (mm^3) measured with MR		*ex vivo* volumes (mm^3) measured with CT		shrink age (%)	P (*in vivo* versus *ex vivo*)
	Mean	SD	Mean	SD	Mean	SD		
Zinc-based fixative (6 h)	315	3	428.7	10.1	358.1	30.8	16.5	=0.029
Zinc-based fixative (24 h)	315	3	429.2	19.7	342.0	29.1	20.3	<0.001
Zinc-based fixative (48 h)	315	3	455.4	15.0	303.0	18.0	33.5	<0.001
NBF (48 h)	1695	10	489.6	8.3	202.9	18.6	58.6	<0.001
NBF (48 h) diluted*	264	1	487.4	26.0	332.5	0.4	31.8	=0.009
PFA (48 h)	1471	2	495.7	18.3	197.3	17.0	60.2	<0.001
Bouin-Holland fixative (48 h)	1922	34	476.4	9.3	289.5	9.8	39.2	<0.001
PLP (48 h)	969	20	472.9	9.7	150.9	34.4	68.1	<0.001
NaCl (48 h)	293	0	480.5	8.8	419.7	34.0	12.7	=0.072

NBF, neutral buffered formalin; PFA, Paraformaldehyde; PLP, Paraformaldehyde-lysine-periodate; NaCl, isotonic sodium chloride solution; SD, Standard deviation; P, P-value. * NBF diluted: osmolarity adapted to NaCl values by dilution with aqua.

2). The metal ion-based fixatives (zinc for zinc-based fixatives, copper for Bouin-Holland fixative) revealed higher density values compared to the formalin-based fixatives (PFA, PLP). Interestingly, the HU density values for the zinc-based fixatives steadily progressed from -59.5 (6 h) to 60.6 (48 h). This is also reflected by Fig. 2A,B. While the rim areas of the paraffin-embedded brains appear hyper-dense after 6 h (Fig. 2A) and 12 h (Fig. 2B) zinc-based fixation, the brain core areas show a lower density after 6 h (Fig. 2A). However, there still remains a density gradient between brain rim and core even after 48 h fixation. This is also reflected by a radiodensity profile between the right to the left temporal lobes (Fig. 2C). While the temporal cortex

Table 2. *Ex vivo* brain tissue radiodensity values of the different fixative groups.

	ex vivo radiodensity (HU)	
	Mean	SD
Zinc-based fixative (6 h)	-59.5	16.1
Zinc-based fixative (24 h)	36.3	11.7
Zinc-based fixative (48 h)	60.6	22.0
NBF (48 h)	-100.9	10.3
PFA (48 h)	-143.4	8.1
Bouin-Holland fixative (48 h)	36.9	11.8
PLP (48 h)	-137.3	57.5

HU, Hounsfield units; NBF, neutral buffered formalin; PFA, Paraformaldehyde; PLP, Paraformaldehyde-lysine-periodate; a.u., arbitrary unit; SD, Standard deviation.

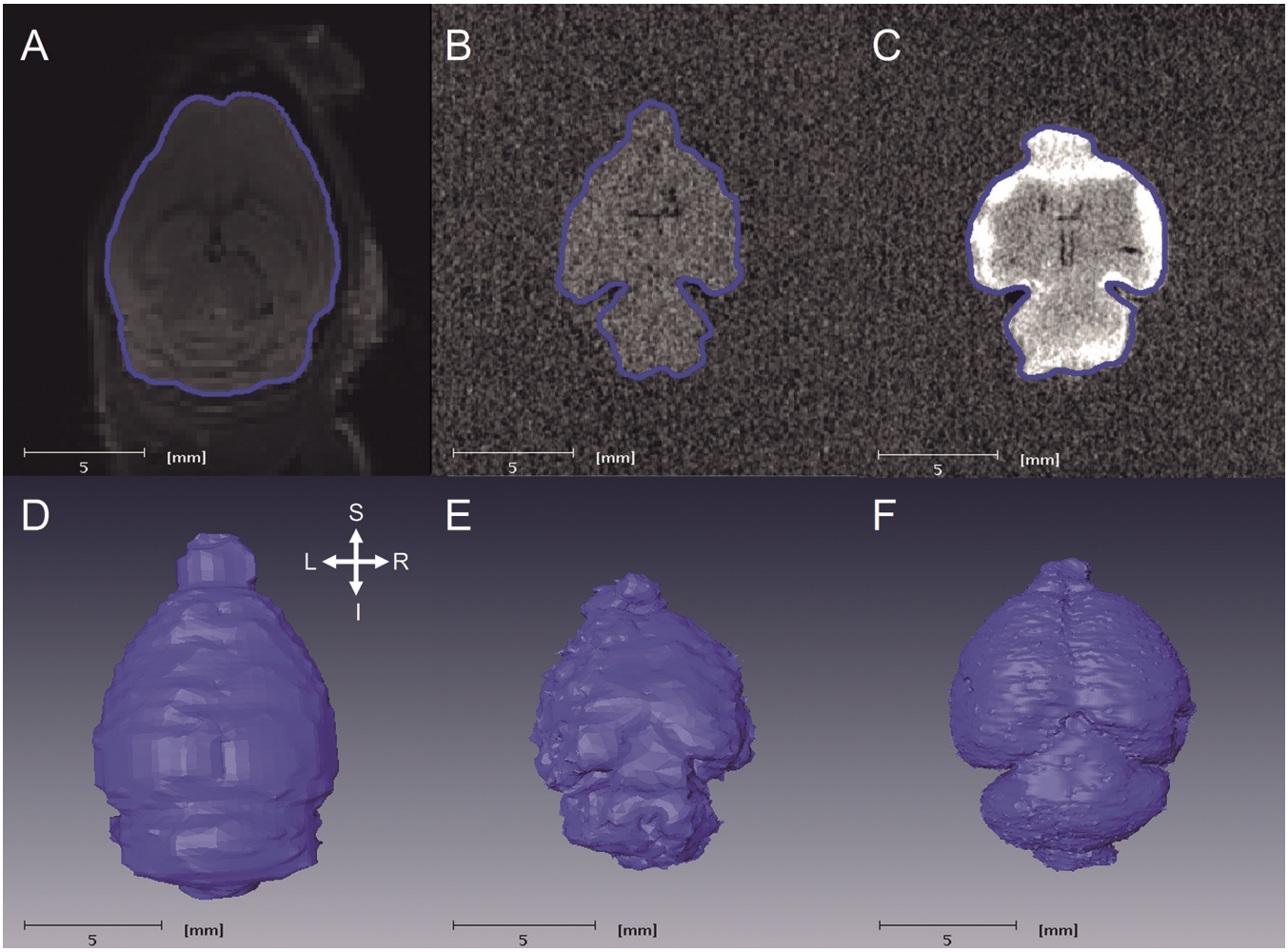

Fig. 1. Comparison of *in vivo* MR and *ex vivo* CT images. **A.** Example of a segmented *in vivo* MR scan of a mouse brain. The high soft tissue contrast of MRI provides detailed information about the brain structures. **B.** Example of a segmented *ex vivo* CT scan of a paraffin-embedded brain after 48 h fixation with PFA. Shrinkage and deformation are clearly present when comparing the CT scan with **A**. **C.** Example of a segmented *ex vivo* CT scan of a paraffin-embedded brain after 48 h fixation with zinc-based fixation. Especially for the brain width, shrinkage is less pronounced compared to **B**. In addition, zinc-based fixation causes higher brain tissue density values resulting in a brighter appearance. **D.** Three-dimensional rendered volume of the segmented *in vivo* MR brain scan. **E.** Three-dimensional rendered volume of **B**. Not only shrinkage of the brain tissue can be observed, but also an irregular brain surface is observed. **F.** Three-dimensional rendered volume of the segmented *ex vivo* CT scan of a paraffin-embedded brain after 48 h fixation with zinc-based fixation. The brain surface is smoother compared to the PFA fixation. Viewing directions are indicated by the arrowed crosshair: L: left, R: right, S: superior (frontal), I: inferior (caudal).

exhibits high-density values on each side, the density decreases towards the central brain structure, especially for the lateral ventricles. Density values for the MR images are not comparable, and therefore not calculated, to the CT radio density values, since both methods are based on different physical tissue properties.

Co-registration of in vivo MR and ex vivo CT images

Fig. 3A,B show rigid co-registrations of MR images (grey) and CT images (red) after 48 h PFA (Fig. 3A) and zinc-based fixation (Fig. 3B). Figure 3A clearly reflects the higher amount of tissue shrinkage and deformation

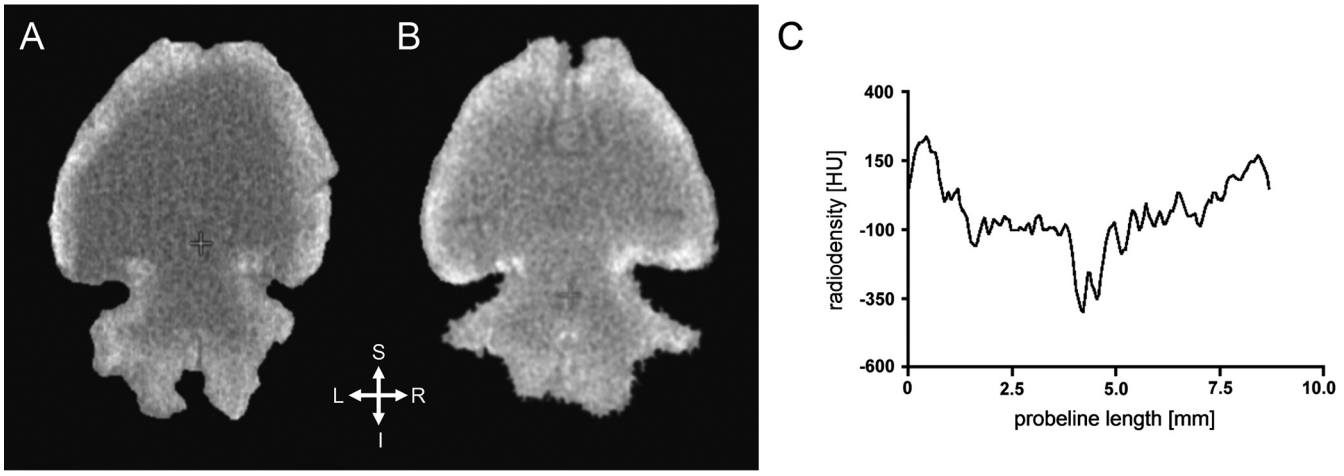

Fig. 2. Tissue density after fixation. **A.** Example of an *ex vivo* CT scan of a paraffin-embedded brain after 6 h zinc-based fixation. The CT scan reveals a higher tissue density at the brain rim compared to the core. **B.** Example of an *ex vivo* CT scan of a paraffin-embedded brain after 12 h zinc-based fixation. After 12 h fixation the difference between rim and core is less pronounced compared to **B**. **C.** Tissue density profile from the right to the left temporal lobe after 48 h zinc-based fixation. Even after 48 h fixation a higher density and consecutively higher accumulation of zinc ions in the brain rim is present. Viewing directions are indicated by the arrowed crosshair: L: left, R: right, S: superior (frontal), I: inferior (caudal).

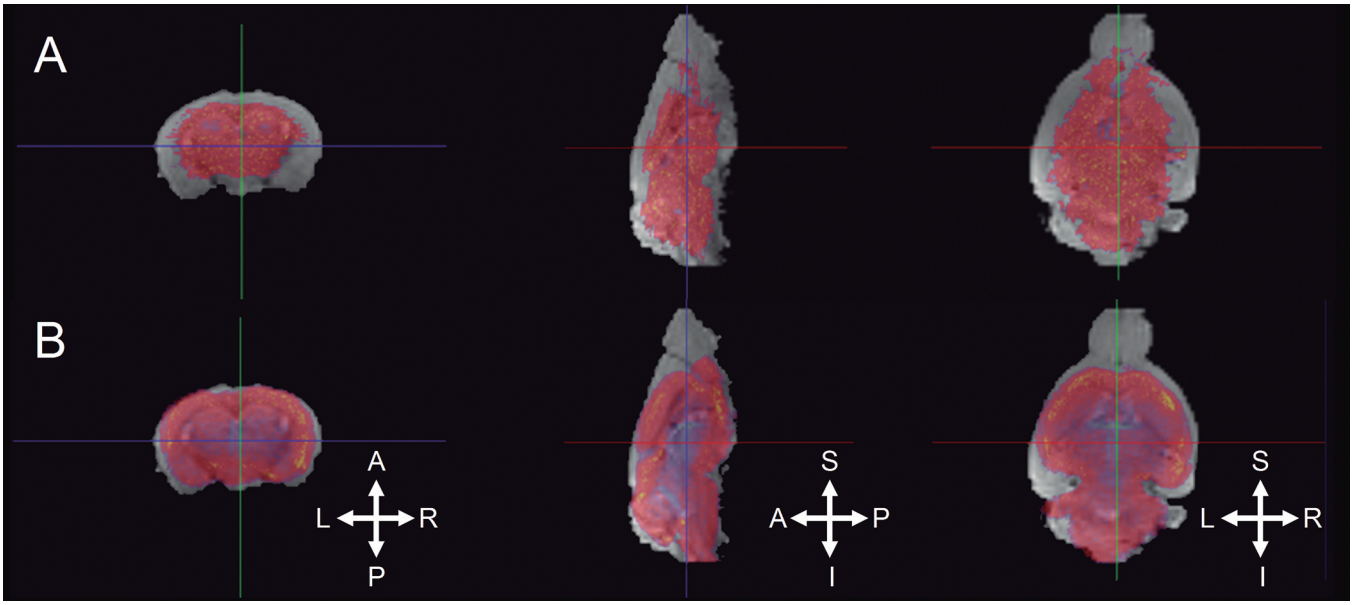

Fig. 3. Comparison of co-registration accuracy. **A.** Co-registration of *in vivo* MR (grey) and *ex vivo* CT (yellow representing high radiodensity, red relatively medium radiodensity and blue representing relatively lower radiodensity values) images after 48 h fixation with PFA. The image fusion clearly reveals a significant shrinkage and deformation of the PFA fixation. **B.** Co-registration of *in vivo* MR and *ex vivo* CT images after 48 h fixation with zinc-based solution. Following zinc-based fixation deformation and shrinkage are less pronounced. Viewing directions are indicated by the arrowed crosshair: A: anterior, P: posterior, L: left, R: right, S: superior (frontal), I: inferior (caudal).

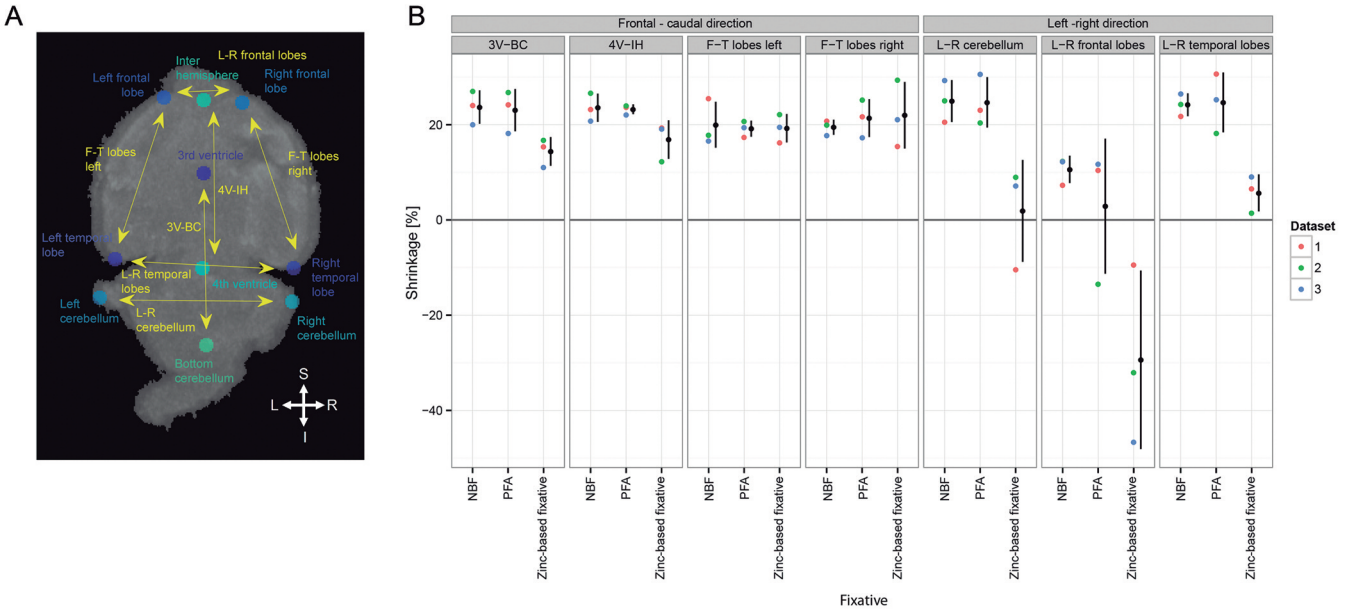

Fig. 4. Landmark-based evaluation of deformation. **A.** Maximum intensity projection of a sample CT dataset with landmarks (blue-green) used for landmark-based shrinkage evaluation. Yellow arrows denote the evaluated distances: 3rd ventricle - bottom cerebellum (3V-BC), 4th ventricle - interhemisphere (4V-IH), frontal-temporal lobes left and right (F-T lobes left and right), left cerebellum - right cerebellum (L-R cerebellum), left frontal lobe - right frontal lobe (L-R frontal lobes), left temporal lobe - right temporal lobe (L-R temporal lobes). **B.** Shrinkage of the evaluated distances for the respective fixatives (NBF, PFA and zinc-based each for 48 h). Black dots and lines denote the mean and standard deviation. Viewing directions are indicated by the arrowed crosshair: L: left, R: right, S: superior (frontal), I: inferior (caudal).

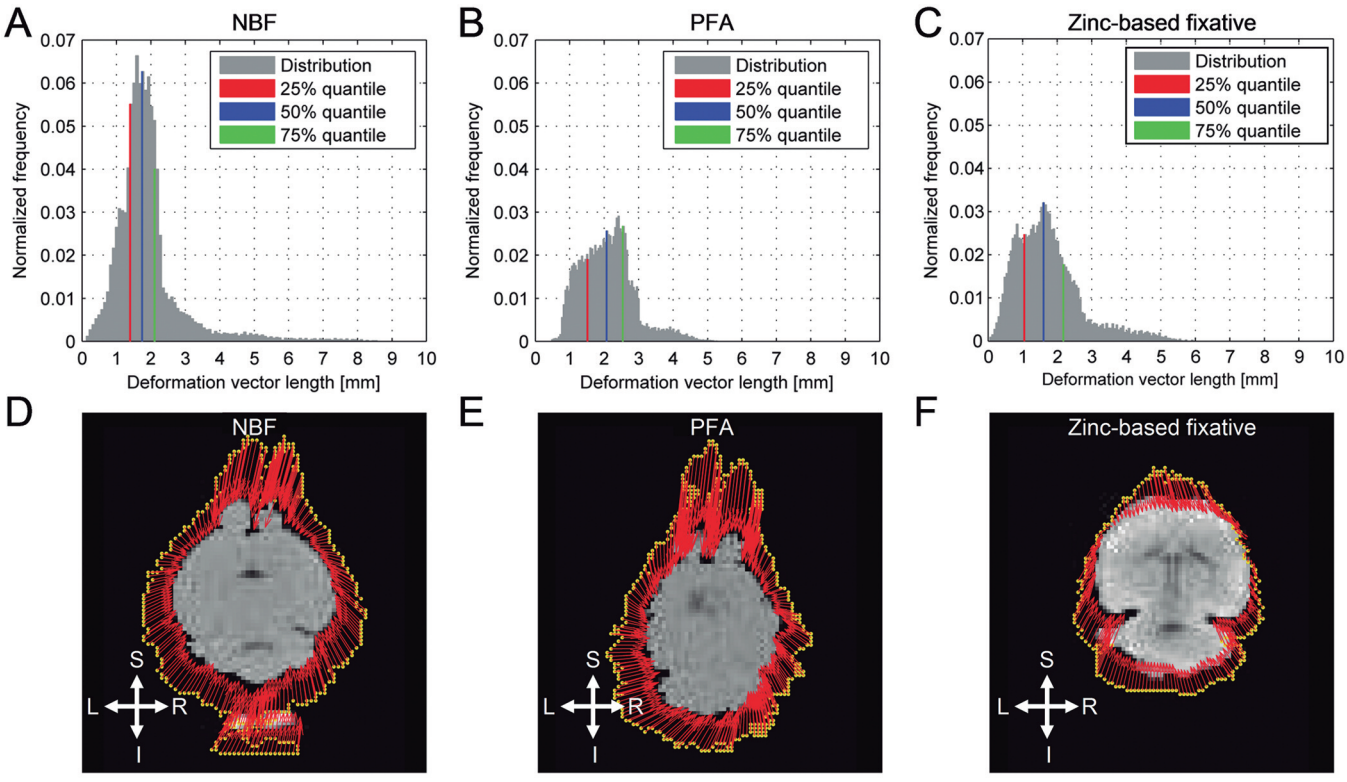

Fig. 5. Distributions of surface deformation vector lengths for deformable registrations between *in vivo* and *ex vivo* images. **A-C.** Histograms of the deformation vector length distributions for deformable registrations between *ex vivo* CT and *in vivo* MR datasets for the fixatives NBF, PFA and zinc-based, each for 48 h. **D-F.** Corresponding contour deformations for a single *ex vivo* CT slice of representative datasets. Yellow dots denote the contour of the corresponding slice in the *in vivo* MR image. Red arrows show the deformation vector. Viewing directions are indicated by the arrowed crosshair: L: left, R: right, S: superior (frontal), I: inferior (caudal).

resulting from PFA fixation. Figure 3B indicates that the zinc-based fixation also undergoes some degree of shrinkage, although the brain morphology does in general fit more closely to the original *in vivo* imaging data.

Landmark-based evaluation of brain tissue shrinkage

We observed shrinkage levels (Fig. 4) for frontal-caudal distances between landmarks in the inner regions of the brain (3V-BC, 4V-IH) in the range of 11.0%-27.0%. The zinc-based fixative (48 h) showed lower mean shrinkage levels (14.4% and 16.9%) than NBF (48 h) and PFA (48 h) (23.1%-23.7%). For distances based on landmarks placed near the brain surface (F-T lobes left, F-T lobes right) the shrinkage levels were in the range of 15.5%-29.4%, with similar mean shrinkage values for all evaluated fixatives (NBF, PFA, zinc-based fixative) between (19.2%-22.0%).

For left-right distances of landmarks in the caudal regions near the surface (L-R cerebellum and L-R temporal lobes), shrinkage levels were in the range of 20.5%-29.3% for NBF, 18.2%-30.7% for PFA and -10.4%-9.1% for the zinc-based fixative. The mean shrinkage values were lower for the zinc-based fixative (1.9% for L-R cerebellum and 5.7% for L-R temporal lobes) than for NBF and PFA in these areas (24.2%-25.0%). For the left-right distance in the frontal brain region (L-R frontal lobes), the shrinkage levels were in the range of 7.3%-12.3% for NBF, -13.5% - -11.7% for PFA and -46.7% - -9.5% for the zinc-based fixative. Negative shrinkage levels, i.e. an increase in distance, were observed for PFA and zinc-based fixative.

Deformable registration-based evaluation of brain tissue shrinkage

Figure 5A-C show the histograms of the deformation vector length distribution for NBF, PFA and zinc-based fixative for 48 h fixation time, respectively. Figure 5D-F represents the corresponding contour deformations for a single slice of representative datasets.

The distribution of deformation vector lengths for NBF (Fig. 5A) exhibits a pronounced concentration around the median value (50% quantile) of 1.74 mm, with values of 1.39 mm and 2.11 mm for 25% and 75% quantiles, respectively. PFA showed a broad distribution (Fig. 5B) with the highest values for each quantile of the three evaluated fixatives (1.52 mm, 2.07 mm and 2.54 mm for 25%, 50% and 75% quantiles). The zinc-based fixative showed the lowest 25% and 50% quantile values (Fig. 5C) of 1.05 mm and 1.61 mm, respectively. The distribution showed a higher spread than NBF, the value of the 75% quantile was higher with 2.18 mm compared to 2.11 mm for NBF.

The peakedness, lack of shoulders of the respective distributions can be described by the kurtosis value, where a low kurtosis represents a broad distribution of the deformation vector length values, indicating a non-linear tissue deformation. For NBF we found a kurtosis value of 12.8, for PFA 3.7 and for the zinc-based fixative 4.7, indicating that NBF has the lowest spread of deformation vector lengths (i.e most deformation vector lengths are similar), whereas PFA and the zinc-based fixative exhibit a broader distribution (i.e. a larger variety of deformation vector lengths). This inhomogeneity of tissue surface deformation due to fixation is exemplarily shown in Figure 6 for the zinc-based fixative.

Histology

Figure 7 shows representative coronal (imaging slice orientation, in histological context this orientation is often referred as horizontal) mouse brain tissue sections from the midbrain with H&E staining (Fig. 7A-C 200x,

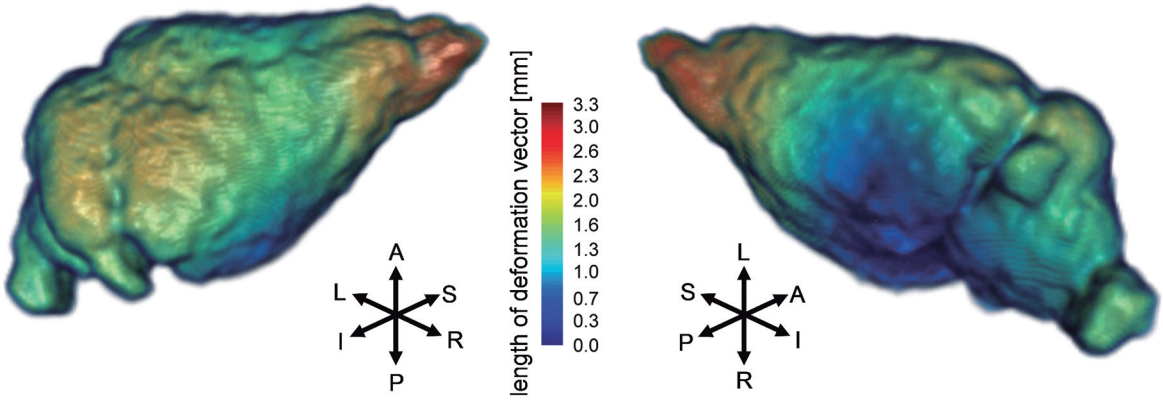

Fig. 6. Visualization of inhomogeneous surface deformation. Length of the surface deformation vectors for the zinc-based fixative (48 h) for a sample dataset, projected onto the corresponding *ex vivo* CT image, presented as a three-dimensional volume rendering. Left: oblique top view, right: oblique bottom view. The median deformation of this dataset is 1.82 mm. Anisotropic deformation due to fixation can be observed, with the highest degree found in the cerebellar and bulbic areas. Lower degrees of deformations are observed in the hypothalamic and pons areas. Viewing directions are indicated by the arrowed crosshair: A: anterior, P: posterior, L: left, R: right, S: superior (frontal), I: inferior (caudal).

Fig. 7D-F 400x) and GFAP immunohistochemistry (Fig. 7G-I 200x). Tissue fixations with NBF (Fig. 7A,D) and PFA (Fig. 7B,E) provide an advantageous preservation of the morphology with clear delineation of the cell cytoplasm and nuclei, as well as the extracellular matrix. Figure 7C and F present an example after zinc-based fixation. Both examined brains that were fixed in zinc-based fixative showed typical signs of shrinkage better seen at higher magnification x 400, such as a retraction artifact, appearing as empty spaces, so called pericellular halos. GFAP immunohistochemistry is shown for all three fixatives (Fig. 7G-I). The histological quality of the tissues fixed in zinc-based fixative is not as good as the quality of tissues fixed in NBF and PFA.

Discussion

Our results reveal that a zinc-based fixative causes overall smaller tissue shrinkage artifacts, compared to more traditional fixatives such as formalin solutions. This is of special interest for *in vivo* to *ex vivo* comparison studies.

In the past decades, many different tracers and biomarkers for non-invasive *in vivo* imaging of neurological disease have been developed and a correlation as well as validation based on histology is

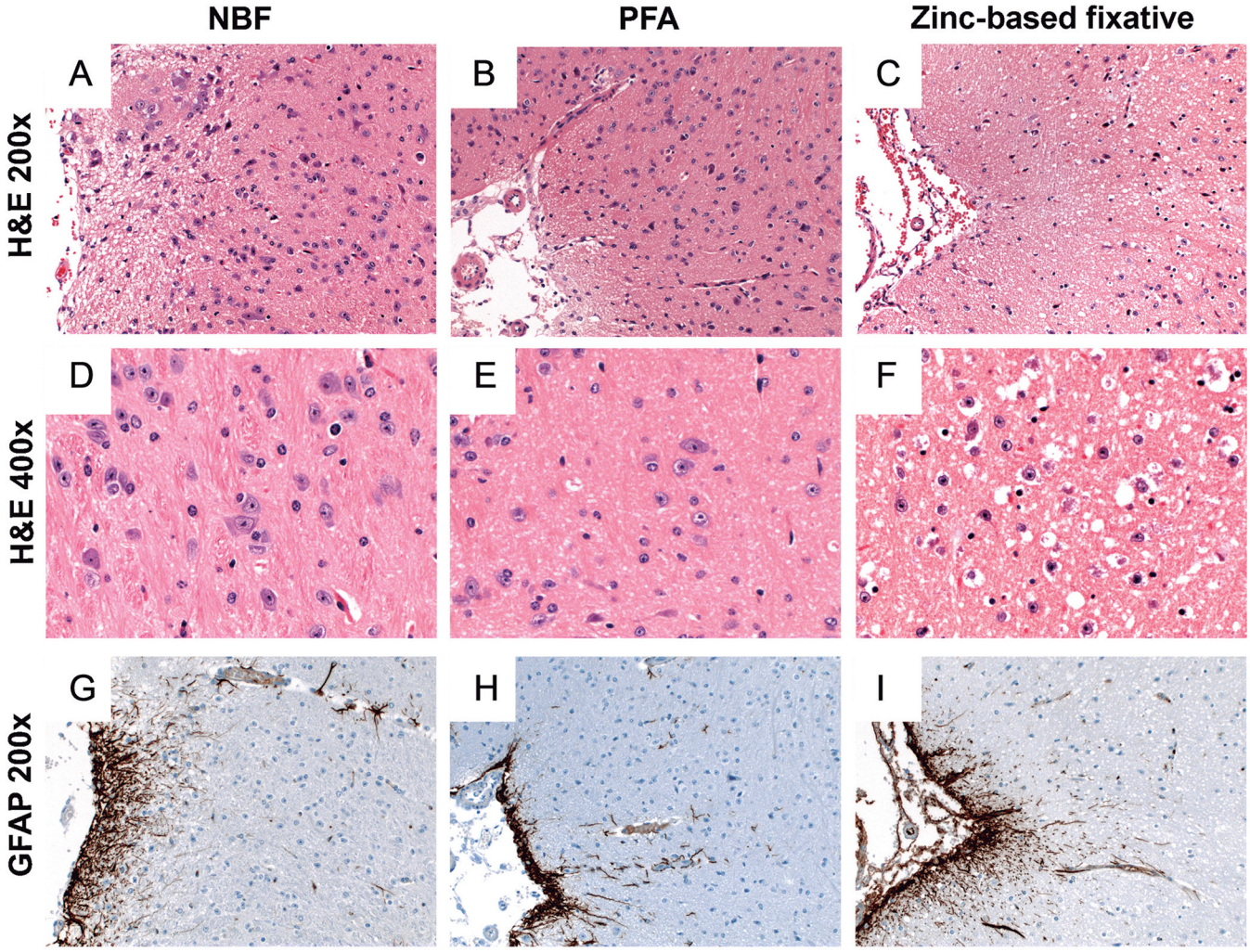

Fig. 7. Assessment of the fixation effects on the quality of histology and morphology. **A** Hematoxylin and eosin (H&E) staining of an axial midbrain tissue section after NBF fixation, after PFA fixation **(B)** and after zinc-based fixation **(C)**. Higher magnification demonstrates high quality tissue fixation with NBF **(D)** and PFA **(E)**, as indicated by good preservation of the cell cytoplasm, nuclei and extracellular matrix. **F.** H&E staining of an axial midbrain tissue section after zinc-based fixation. Zinc-based fixation showed typical signs of shrinkage better visualized at higher magnification, such as retraction artifact, appearing as empty spaces, so called pericellular halos. In addition, the cells show hyperchromatic nuclei with poor cytological definition. Glial fibrillary acidic protein (GFAP) immunohistochemistry of an axial midbrain tissue section after NBF fixation **(G)**, PFA fixation **(H)**, and zinc-based fixation **(I)**. In summary, the histological quality of the tissues fixed in zinc-based fixative is not as good as NBF and PFA. A-C, G-I, x 200; D-F, x 400.

highly important (Small, 2005; Buongiorno et al., 2011; Willis et al., 2012). The number of volumetric studies in the literature considering the effect of dehydration and paraffin embedding is limited and so far only formalin was used as fixative.

MR imaging provides a superior soft tissue contrast compared to other imaging modalities, even in the absence of a contrast agent (Wehrl et al., 2010). In small animal imaging, non-contrast enhanced CT barely shows the outline of the animal brain and other structures (Wehrl et al., 2010). MRI uses in most cases the signal from hydrogen protons, which are found in a vast majority of biomolecules, especially water – which is an important part of many tissue compositions. Especially for brain imaging studies, *in vivo* small animal MRI is often the method of choice, mainly due to its superior soft tissue contrast compared to CT. However, in dehydrated tissues, spin-lattice relaxation times (T1) and spin-spin relaxation times (T2) are lower compared to normal tissues (Brown et al., 1984). In our study, the water signal was so much reduced because of the histological processing and also the paraffin embedding that MR imaging was not feasible even when using a 7 T magnetic field - this was also reflected by an *ex vivo* MR image quality that was too low to reliably determine tissue boundaries and outlines using the imaging sequence used for the *in vivo* images. Recently, MR techniques e.g. based on ultra short echo times (UTE), have been used to detect signals from materials with low water content (Sharma et al., 2010). However, such UTE techniques require specialized MR hardware, sequences and often deliver very special contrast properties, which are not comparable to standard anatomical T1 or T2 weighted MR sequences, which are often favorable for the assessment of brain tissue und structure. Moreover, UTE techniques can suffer from spatial distortions (Du et al., 2008) that make an assessment of geometrical deformations difficult. Therefore, *ex vivo* imaging of the paraffin-embedded brain samples was performed using a CT. MRI and CT imaging allow an acquisition of isotropic, three-dimensional datasets. Subsequently, sectioning of the brains is not required, which further reduces artifacts. Additionally, volumes calculated from imaging data might not be as error-prone as those derived from macroscopic caliper measurements or planimetry, as already demonstrated for subcutaneous tumors (Jensen et al., 2008). Given the restrictions on the choice of imaging modality used, our compromise, to use *in vivo* MRI, which appears to be most suitable for living soft tissue contrast, and *ex vivo* CT, which appears to be most suitable for non destructive, distortion free sample imaging, is reasonable. It also mimics the situation often encountered in small animal imaging, where *in vivo* MR images are compared with *ex vivo* histology - and it is just this degree of *ex vivo* histological alterations that are assessed by the *ex vivo* CT imaging.

Considering the first step of post mortem tissue preparation, already fixation e.g. in formalin causes deformations. The effects of formalin on the human brain have been shown to cause a maximum increase in weight and volume between day 1 and 5 (Quester and Schröder, 1997). This weight increase is 7.0-13.4% for 4% formalin (Quester and Schröder, 1997). After several weeks and months weight and volume subsequently decrease (Quester and Schröder, 1997). Schulz et al. calculated a global volume shrinkage of 8.1% over a period of 70 days of human brains still within the cranium (Schulz et al., 2011). It was shown that the dehydration in ethyl alcohol produces a strong decrease of volume and weight from 32-39% of the fresh brain weight (Wegiel et al., 1989). Studies found a mean shrinkage in paraffin embedded sections of 42%-51% depending on the part of the brain (Gellért and Csernovszki, 1971; Mouritzen, 1979; Kretschmann et al., 1982). In this study we have investigated comparable results for our PFA 48 h fixative group with 60.2% shrinkage and 58.6% shrinkage for the NBF group. The highest degree of shrinkage was observed with PLP fixation, containing 8% formalin, resulting in 68.1% shrinkage. The zinc-based fixatives revealed a time-dependency with 16.5% after 6 h, 20.3% after 24 h and 33.5% after 48 h. The Bouin-Holland fixative, which is also based on metal ions, revealed 39.2%. The osmolarity values range from 1922±34 mOsmol/kg for the Bouin-Holland fixative to 264±1 mOsmol/kg for the diluted NBF. We observed a tendency to higher shrinkage rates for fixatives having an osmolarity that greatly differs from the osmolarity of normal extracellular fluid (293±34 mOsmol/kg using the values for NaCl as an approximation). Loqman et al. could markedly reduce the shrinkage artifact by adjusting the osmolarity of their fixatives to the osmotic pressure of normal extracellular fluids (Loqman et al., 2010). However, our results suggest a non-linear relationship between osmolarity values and observed shrinkage. E.g. for the Bouin-Holland fixative we observed the highest osmolarity (1922 mOsmol/kg) but only a shrinkage of 39.2%, whereas for PFA which has an osmolarity of 1471 mOsmol/kg a higher shrinkage value of 60.2% was measured. Also, the diluted NBF fixative with an osmolarity close to NaCl still caused shrinkage of 31.8%. We therefore conclude that the osmolarity of the fixatives is not the only factor influencing the shrinkage of the entire embedded structure. The discrepancy with the observations made by Loquman et al. can be resolved by the fact that they focused on the shrinkage on a cellular level, whereas this work measures the shrinkage on a global, entire embedded organ (brain) level. Furthermore, the additional steps in the fixation process, such as the ethanol gradient and paraffin embedding can have an influence on the tissue shrinkage. The difference between *in vivo* brain volumes and *ex vivo* brain volumes measured directly after resection of the brains from the skull was not significant. Therefore, the effect of the skull alone on the brain volume change observed is negligible. Interestingly, not only the volumes but also the tissue density changed

depending on the fixation type. While the formalin-based fixations showed low-density values of -143.4 HU for PFA (48 h), -137.3 HU for PLP (48 h) and -100.9 HU for NBF (48 h), the Bouin-Holland fixative (48 h) caused high values of 36.9 HU. For the zinc-based fixatives a time-dependency for the tissue density was found: 6 h (-59.5 HU), 24 h (36.3 HU), 48 h (60.6 HU). These increasing densities are probably linked to the accumulation of zinc or copper ions in the tissue, although a direct measurement of zinc or copper concentrations was not performed. CT is an excellent tool for the non-invasive measurement of tissue density (Rutt et al., 1985). The increased tissue density can simplify the segmentation of the brain CT scan by the application of threshold-based methods (Juergens et al., 2008). Fixation for 6 h in zinc-based solution might be sufficient for small tissue samples and we could detect a higher radiodensity in the rim of the brain, which might indicate an accumulation of zinc ions in this region, although in general a fixation time of at least 24 h is recommended (Lykidis et al., 2007).

The comparison of distances between landmarks confirmed the overall results for the degree of shrinkage and additionally revealed a higher degree of shrinkage for the zinc-based fixative in the frontal-caudal direction (11%-29.4%) than in left-right direction (-46.7%-9.1%) for the zinc-based fixative. The increase in distances (negative shrinkage) can be probably attributed to the location of the landmarks at the surface near the frontal lobes (Fig. 4A). The observed reduction of the distance between frontal and temporal lobes leads to the translation of the L-R frontal lobe landmarks along the brain surface, so that the distance reduction is to some extent offset by deformation. Additionally, the degree of the offset might be dependent on the type of fixative and the degree of its interaction with the local tissue. The histograms of deformation vector lengths for NBF showed the most peaked distribution, indicated by the high kurtosis value, suggesting a more homogeneous shrinkage in all directions in comparison to PFA or zinc-based fixatives. However, shrinkage inhomogeneity for zinc-based fixative (kurtosis 4.7) is comparable with PFA (kurtosis 3.7). Moreover, the zinc-based fixative shows the lowest median value of 1.61 mm for the deformation vector length and also on average the lowest shrinkage between landmarks.

The histological evaluation proved that NBF, PFA and zinc-based fixatives are suited for H&E staining as well as for immunohistochemistry as exemplarily demonstrated by the GFAP. However, the zinc-based fixative shows in H&E staining a perinuclear retraction artifact, which needs to be taken into account when analyzing images, therefore the histological quality of tissues fixed in NBF and PFA is better compared with tissues fixed in zinc-based fixatives.

Our study has several limitations. First, volumetric measurements were only carried out by one reader and with two different imaging modalities. However, the discussed histological data on tissue shrinkage found in the literature are mainly based on caliper measurements and were also carried out by only one reader. It is known that intra- and interobserver agreement for the segmentation of brain lesions on MRI is quite good (Fiez et al., 2000). Regarding cross-modality concordance between CT and MR brain imaging, a good agreement can be found (Robertson et al., 2003). Next, we have segmented only the whole brain including cerebrum and cerebellum, but not different areas separately. According to Weisbecker, who studied mouse brains, formalin fixation leads to an immediate distortion of the brains towards a stouter shape - with an anisotropic distortion related component accounting for 26% of overall variation including isotropic size change (Weisbecker, 2012). This group described also that the anisotropic distortion might have stronger effects on wider and stouter brain dimensions, although in certain areas such as the cerebellum a smaller shape change was observed (Weisbecker, 2012). However, the goal of our study was to compare the effects of fixation and paraffin-embedding in more general terms. Also, the use of a deformable image registration between different image modalities to evaluate the length of the surface deformation vectors has some limitations. Errors in the registration affect the deformation vector lengths, as shown in Figure 5F, where the frontal contour is not exactly matched. However, the registration errors affect all datasets, thus we expect no significant bias for one particular fixative. Moreover, gravitational effects may also account for the observed deformation. These might be reduced by the use of suspensions or fixatives with higher densities. Given the differences of relative brain weight and relative brain cross sectional area between humans and mice (Defelipe, 2011), and assuming similar tissue elastic properties, the gravitational effect should be less pronounced in mice compared to human brain tissue samples. However, since the tissue handling was the same for all studied fixatives, the gravitational bias should be the same for all tissues and fixatives studied.

It should be noted, that besides what was investigated, mostly formalin and zinc-based fixatives, other alternative fixatives and technologies exist (Kacena et al., 2004; Vollmer et al., 2006; Ozkan et al., 2012). A thorough investigation of these fixatives and technologies in respect to their suitability for *in vivo* to *ex vivo* comparison studies is certainly needed. The shrinkage artifacts observed in formalin based fixatives have also a clinical impact, because they can e.g. interfere with the evaluation of the tumor-free margin in certain specimens (Docquier et al., 2010).

In conclusion, we could show that shrinkage degree is strongly dependent on the fixation type. Compared to NBF, the zinc-based fixative shows a larger degree of inhomogeneity in tissue shrinkage, but is still more homogenous than PFA. The perinuclear retraction artefact seen in H&E staining of zinc-based fixative sections needs to be considered when analyzing histological section. Given our findings, it is obvious that a compromise between tissue shrinkage,

inhomogeneity of shrinkage and suitability of histological staining has to be made when considering the evaluated fixatives.

Conflict of Interest. Bernd J. Pichler receives grant/research support from Siemens, AstraZeneca, Bayer Healthcare, Boehringer-Ingelheim, Oncodesign, Merck, Bruker and the Werner Siemens-Foundation. The other authors have no potential conflict of interest.

Acknowledgements. These studies were supported by funding from the Werner Siemens-Foundation, Zug, Switzerland, the Eberhard Karls University, Tuebingen, Germany (fortüne 1918-0-0 and fortüne 2209-0-0: "Functional and Metabolic Brain Imaging (FMBI)") and the German Research Foundation (DFG PI 771/5-1). Sources of support that require acknowledgement: Werner Siemens-Foundation, Zug, Switzerland; Eberhard Karls University, Tuebingen, Germany (fortüne 1918-0-0); Eberhard Karls University, Tuebingen, Germany (fortüne 2209-0-0: "Functional and Metabolic Brain Imaging (FMBI)"); German Research Foundation (DFG PI 771/5-1)

References

Benerini Gatta L., Cadei M., Balzarini P., Castriciano S., Paroni R., Verzeletti A., Cortellini V., De Ferrari F. and Grigolato P. (2012). Application of alternative fixatives to formalin in diagnostic pathology. Eur. J. Histochem. 56, e12.

Brown J.J., Andre M.P. and Slutsky R.A. (1984). Proton nuclear magnetic resonance tissue analysis of normal, volume overloaded, and dehydrated rabbit myocardium. Am. Heart J. 108, 159-164.

Buongiorno M., Compta Y. and Martí M.J. (2011). Amyloid-β and τ biomarkers in Parkinson's disease-dementia. J. Neurol. Sci. 310, 25-30.

Defelipe J. (2011). The evolution of the brain, the human nature of cortical circuits, and intellectual creativity. Front. Neuroanat. 5, 29.

Docquier P.L., Paul L., Cartiaux O., Lecouvet F., Dufrane D., Delloye C. and Galant C. (2010). Formalin fixation could interfere with the clinical assessment of the tumor-free margin in tumor surgery: magnetic resonance imaging-based study. Oncology 78, 115-124.

Dorph-Petersen K.A., Nyengaard J.R. and Gundersen H.J. (2001). Tissue shrinkage and unbiased stereological estimation of particle number and size. J. Microsc. 204, 232-246.

Du J., Bydder M., Takahashi A.M. and Chung C.B. (2008). Two-dimensional ultrashort echo time imaging using a spiral trajectory. Magn. Reson. Imaging 26, 304-312.

Eltoum I., Fredenburgh J. and Grizzle W.E. (2001). Advanced concepts in fixation: 1. Effects of fixation on immunohistochemistry, reversibility of fixation and recovery of proteins, nucleic acids, and other molecules from fixed and processed tissues. 2. Developmental Methods of Fixation. J.Histotechnol. 24, 201-210.

Fiez J.A., Damasio H. and Grabowski T.J. (2000). Lesion segmentation and manual warping to a reference brain: intra- and interobserver reliability. Hum. Brain Mapp. 9, 192-211.

Gellért A. and Csernovszki E. (1971). Anwendung der Paraffintechnik bei der Herstellung anatomischer Präparate. Aus einem Nachlass-Material zusammengestellt. Studia medica Szegedinensia, 8, 24.

Howat W.J. and Wilson B.A. (2014). Tissue fixation and the effect of molecular fixatives on downstream staining procedures. Methods 70, 12-19.

Jensen M.M., Jorgensen J.T., Binderup T. and Kjaer A. (2008). Tumor volume in subcutaneous mouse xenografts measured by microCT is more accurate and reproducible than determined by 18F-FDG-microPET or external caliper. BMC Med. Imaging 8, 16.

Juergens K.U., Seifarth H., Range F., Wienbeck S., Wenker M., Heindel W. and Fischbach R. (2008). Automated threshold-based 3D segmentation versus short-axis planimetry for assessment of global left ventricular function with dual-source MDCT. AJR Am. J. Roentgenol. 190, 308-314.

Kacena M.A., Troiano N.W., Coady C.E. and Horowitz M.C. (2004). HistoChoice as an alternative to formalin fixation of undecalcified bone specimens. Biotech. Histochem. 79, 185-190.

Kretschmann H.J., Tafesse U. and Herrmann A. (1982). Different volume changes of cerebral cortex and white matter during histological preparation. Microsc. Acta 86, 13-24.

Liu J.-X., Chen Y.-S. and Chen L.-F. (2010). Fast and accurate registration techniques for affine and nonrigid alignment of MR brain images. Ann. Biomed. Eng. 38, 138-157.

Loqman M.Y., Bush P.G., Farquharson C. and Hall A.C. (2010). A cell shrinkage artefact in growth plate chondrocytes with common fixative solutions: importance of fixative osmolarity for maintaining morphology. Eur. Cell. Mater 19, 214-227.

Lykidis D., Van Noorden S., Armstrong A., Spencer-Dene B., Li J., Zhuang Z. and Stamp G.W. (2007). Novel zinc-based fixative for high quality DNA, RNA and protein analysis. Nucleic Acids Res. 35, e85.

Mouritzen D.A. (1979). Shrinkage of the brain during histological procedures with fixation in formaldehyde solutions of different concentrations. J. Hirnforsch. 20, 115-119.

Overgaard K. and Meden P. (2000). Influence of different fixation procedures on the quantification of infarction and oedema in a rat model of stroke. Neuropathol. Appl. Neurobiol. 26, 243-250.

Ozkan N., Salva E., Cakalagaoglu F. and Tuzuner B. (2012). Honey as a substitute for formalin? Biotech. Histochem. 87, 148-153.

Pieri L., Sassoli C., Romagnoli P. and Domenici L. (2002). Use of periodate-lysine-paraformaldehyde for the fixation of multiple antigens in human skin biopsies. Eur. J. Histochem. 46, 365-375.

Quester R. and Schröder R. (1997). The shrinkage of the human brain stem during formalin fixation and embedding in paraffin. J. Neurosci. Methods 75, 81-89.

Robertson R.L., Robson C.D., Zurakowski D., Antiles S., Strauss K. and Mulkern R.V. (2003). CT versus MR in neonatal brain imaging at term. Pediatr. Radiol. 33, 442-449.

Rutt B.K., Stebler B.G., Cann C.E., Boyd D.P., Genant H.K. and Manatt S.L. (1985). Whole-body CT scanner for ultraprecise, ultraaccurate determination of bone density. J. Comput. Assist. Tomogr. 9, 609-610.

Sakanaka M., Shibasaki T. and Lederis K. (1987). Improved fixation and cobalt-glucose oxidase-diaminobenzidine intensification for immunohistochemical demonstration of corticotropin-releasing factor in rat brain. J. Histochem. Cytochem. 35, 207-212.

Schulz G., Crooijmans H.J., Germann M., Scheffler K., Müller-Gerbl M. and Müller B. (2011). Three-dimensional strain fields in human brain resulting from formalin fixation. J. Neurosci. Methods 202, 17-27.

Sharma S., Boujraf S., Bornstedt A., Hombach V., Ignatius A., Oberhuber A. and Rasche V. (2010). Quantification of calcifications in endarterectomy samples by means of high-resolution ultra-short echo time imaging. Invest. Radiol. 45, 109-113.

Shepherd T.M., Thelwall P.E., Stanisz G.J. and Blackband S.J. (2009). Aldehyde fixative solutions alter the water relaxation and diffusion

properties of nervous tissue. Magn. Reson. Med. 62, 26-34.

Small S.A. (2005). Alzheimer disease, in living color. Nat. Neurosci. 8, 404-405.

Tbakhi A., Totos G., Pettay J.D., Myles J. and Tubbs R.R. (1999). The effect of fixation on detection of B-cell clonality by polymerase chain reaction. Mod. Pathol. 12, 272-278.

Vollmer E., Galle J., Lang D.S., Loeschke S., Schultz H. and Goldmann T. (2006). The HOPE technique opens up a multitude of new possibilities in pathology. Rom. J. Morphol. Embryol. 47, 15-19.

Wegiel J., Medyńska E., Dziedziak W., Szirkowiec-Gmurczyk W. and Dymecki J. (1989). Effect of histological technics on the volume and weight of various brain structures of rats at the early stages of life. Neuropatol. Pol. 27, 279-294.

Wehrl H.F., Sauter A.W., Judenhofer M.S. and Pichler B.J. (2010). Combined PET/MR imaging--technology and applications. Technol. Cancer. Res. Treat. 9, 5-20.

Weisbecker V. (2012). Distortion in formalin-fixed brains: using geometric morphometrics to quantify the worst-case scenario in mice. Brain. Struct. Funct. 217, 677-685.

Werner M., Chott A., Fabiano A. and Battifora H. (2000). Effect of formalin tissue fixation and processing on immunohistochemistry. Am. J. Surg. Pathol. 24, 1016-1019.

Wester K., Asplund A., Backvall H., Micke P., Derveniece A., Hartmane I., Malmstrom P.U. and Ponten F. (2003). Zinc-based fixative improves preservation of genomic DNA and proteins in histoprocessing of human tissues. Lab. Invest. 83, 889-899.

Willis G.L., Moore C. and Armstrong S.M. (2012). Breaking away from dopamine deficiency: an essential new direction for Parkinson's disease. Rev. Neurosci. 23, 403-428.

Zanini C., Gerbaudo E., Ercole E., Vendramin A. and Forni M. (2012). Evaluation of two commercial and three home-made fixatives for the substitution of formalin: a formaldehyde-free laboratory is possible. Environ. Health. 11, 59.

Accepted December 11, 2014